Alexandria Engineering Journal (2018) 57, 2559–2566

HOSTED BY

Alexandria University

Alexandria Engineering Journal

www.elsevier.com/locate/aej
www.sciencedirect.com

ORIGINAL ARTICLE

Boundary layer analysis of persistent moving horizontal needle in magnetohydrodynamic ferrofluid: A numerical study

C. Sulochana *, G.P. Ashwinkumar, N. Sandeep

Department of Mathematics, Gulbarga University, Gulbarga 585106, India

Received 19 May 2017; revised 20 August 2017; accepted 29 August 2017
Available online 19 September 2017

KEYWORDS

Thin needle;
Non-uniform heat source/sink;
Ferrofluid;
MHD;
Nanoparticles;
Viscous dissipation

Abstract The boundary layer analysis of a 2D forced convection flow along a persistent moving horizontal needle in electrically conducting magnetohydrodynamic dissipative ferrofluid is investigated. The energy equation is constructed with the Joule heating, variable heat source/sink and dissipation effects. To check the variation in the boundary layer behaviour, we considered the two ferrofluids namely, Fe_3O_4-methanol and Fe_3O_4-water. The reduced system of governing PDEs are solved by employing the R-K process. Computational results of the flow and energy transport are interpreted with the assistance of tabular and graphical illustrations. Increasing the needle size significantly reduces the flow and thermal fields of both nanofluids. In particular, thermal and velocity fields of Fe_3O_4-methanol nanofluid is highly depreciated when equated with the Fe_3O_4-water nanofluid.

1. Introduction

Recent days, the momentum and heat transfer over an inserted solid object has attracted the minds of several investigators because of their significant applications in several industries and engineering areas. Few of them are a hot wire anemometer or covered thermocouple are used to quantify the airflow velocity, used as heat remover from micro scale equipment. In view of these applications, Chamkha and Issa [1] elaborated the impact of heat source/sink and thermophoresis on 2D magnetohydrodynamic flow past a semi-infinite porous flat surface with the non-uniform magnetic field. A similar kind of investigation was carried by Silva and Gosselin [2]. They incorporated an interesting flow geometry for the higher heat transport rates. Further, non-uniform flow of micropolar fluid through a circular cylinder was numerically analysed using Keller-box method by Ali et al. [3]. Later on, several authors (Refs. [4–8]) proposed the mathematical models to understand the momentum and energy transfer over various body shapes such as a parallel plate, vertical cone, circular cylinder, sphere, wedge, and channels.

Geometrically, the non-uniform thickness is one of the important characteristic features of body objects. An occurrence of these studies can be found in space science and industries. Historically, the investigation of flow past an object with variable thickness was initiated by Lee [9] and he discussed the momentum and thermal transport behavior over a needle.

* Corresponding author.
E-mail address: maths.sulochana@gug.ac.in (C. Sulochana).
Peer review under responsibility of Faculty of Engineering, Alexandria University.

http://dx.doi.org/10.1016/j.aej.2017.08.020

Nomenclature

$\bar{u}, \bar{v}$	velocity components in x and $y-$ directions
$\bar{x}, \bar{r}$	cylindrical coordinates, in axial and radial directions
U_0	composite velocity
u_0, u_∞	velocity of the needle and velocity of the main stream
T_0, T_∞	temperature at the surface and ambient
$\overline{c}$	thickness of the needle
$R(\bar{x})$	surface shape of the thin needle
k_f	thermal conductivity of the base fluid
k_s	thermal conductivity of the solid particles
Pr	Prandtl number
M	magnetic field parameter
Ec	Eckert number
A^*	space dependent heat source/sink
B^*	temperature dependent heat source/sink
C_f	skin friction coefficient.
Nu_x	local Nusselt number

Greek letters

τ_w	surface shear stress
θ	dimensionless temperature
ϕ	solid volume fraction
ρ_{nf}	density of the nanofluid
μ_{nf}	dynamic viscosity of the nanofluid
σ_{nf}	electrical conductivity of the nanofluid
ρ_f	density of the base fluid
ρ_s	density of the nanoparticle
v	kinematic viscosity
$(\rho C_p)_{nf}$	specific heat capacity of the nanofluid at constant pressure
$(\rho C_p)_f$	heat capacity of the base fluid at constant pressure
$(\rho C_p)_s$	heat capacity of the nanoparticle
ψ	stream function
η	similarity variable
γ	velocity ratio parameter

Then after, few authors (Narain and Oberoi [10]) extended the Lee [9] work by considering forced convection fluid on a thin needle. Later, Lee et al. [11] examined the mixed convection flow over two different geometries with uniform heat flux. Further, the related type of study was reported by Ahmad et al. [12] for two cases such as assisting flow and opposing flow. Since then, many investigators (Sulochana and Sandeep [13], Khan et al. [14,15] Babu and Sandeep [16]) worked on fluid flow over a thin needle (i.e. non-uniform thickness), slendering sheet, paraboloid of revolution, stretching sheet.

Generally, conventional fluids used in factories such as water, kerosene, transformer oil cannot meet prerequisites of effective thermal conductivity as needed by the industries. The use of solid particles of the range 1–100 nm in conventional fluids improves the thermal conductivity drastically. These minute solid molecules are called nanoparticles. And use of nanoparticles in a conventional fluid is called nanofluid. Scientifically, use of nanomaterial in conventional fluid upgrades the thermal conductivity to a larger extent, at the very first this concept was introduced by Choi [17]. It is well known that two basic models to describe nanofluid characteristics are Buongiorno [18] and Tiwari and Das [19]. To describe the nanofluid behavior Buongiorno [18] introduced a very strange model with incorporating thermophoresis and Brownian motions. The author found that thermophoresis and Brownian motions are more effective among all used slip mechanisms. Some of the authors (Zulfiqar et al. [20], Hassani et al. [21]) used this model to describe the nanofluid behavior. One more model developed by Tiwari and Das [19] is also helpful in describing nanofluid behavior. Again, this model is also being used by Soid et al. [22]. Very recently, Sheikholeslami and Zeeshan [23] numerically examined the impact magnetic field and constant heat flux on the flow of water based CuO nanofluid by using CVFEM. They incorporated KKL model and found that improving buoyancy forces correspondingly decay heat transfer rate.

Moreover, the impact of radiation on MHD flow of viscous, incompressible fluid through a permeable stretching/shrinking surface with nanoparticles was interrogated by Ibrahim and Shankar [24]. Sandeep et al. [25] presented a comparative analysis of three different kinds of fluids (i.e. Jeffrey, Maxwell and Oldroyd-B) over a stretching surface with considering the suction/injection effects. They found that Oldroyd-B nanofluid is largely reactive in improving Nusselt and Sherwood numbers as compared with Jeffrey and Maxwell nanofluids. Wahed et al. [26] elaborated 2D MHD flow of incompressible nanofluid past a continuous moving surface. For this study, they have taken various effects into accounts such as variable thickness, Brownian motion and heat generation. A very good number of articles are available on the topic nanofluid flow over various geometries with different nanoparticles, few of them are [27–34]. Scientifically, the fluids with magnetic nanoparticles are called ferrofluids. These fluids exhibit more thermal conductivity as compared with other ordinary nanofluids. Sandeep [35] examined the impact of an aligned magnetic field on the flow magnetic-nanofluids (ferrofluids) over a stretched surface. Recently, Sheikholeslami [36] discussed the impact of Coulomb forces on the flow of water based Ferro fluids for the thermal enhancement.

In this analysis, we incorporated the Tiwari and Das model [19] to investigate the boundary layer analysis of a 2D forced convection flow along a persistent moving horizontal needle in electrically conducting magnetohydrodynamic dissipative ferrofluid. To check the variation in the boundary layer behavior, we considered the two ferrofluids namely, Fe_3O_4-methanol and Fe_3O_4-water. The reduced system of governing PDEs are solved by employing the R-K based shooting process.

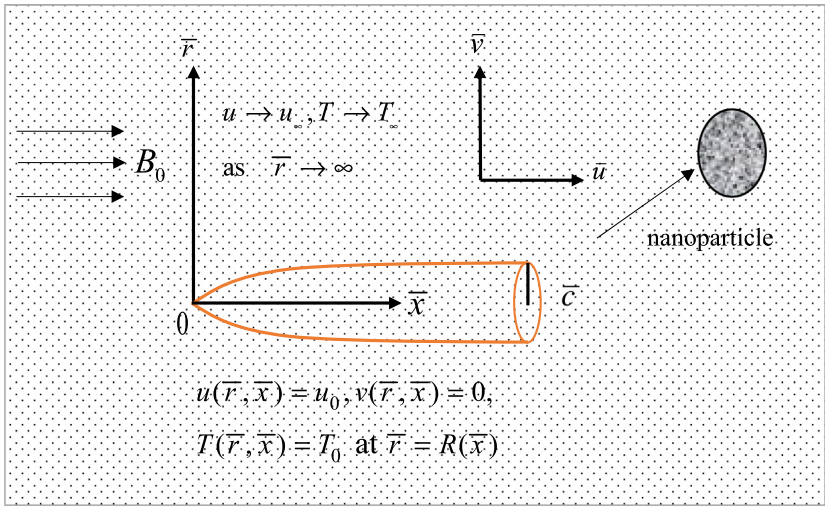

Fig. 1 Flow geometry.

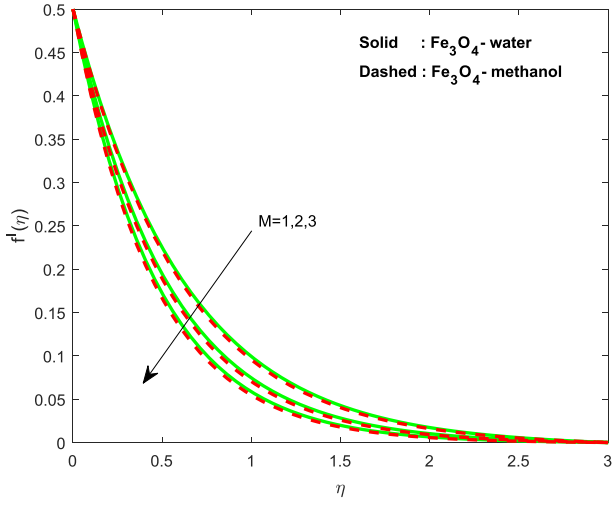

Fig. 2 Velocity behavior with Magnetic field parameter M.

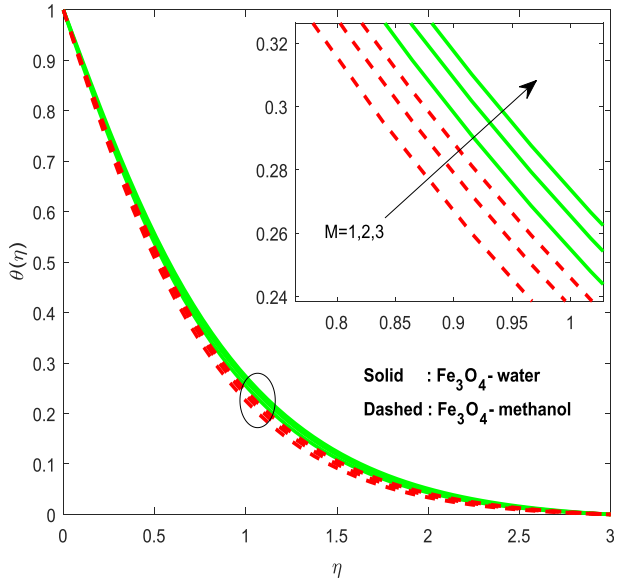

Fig. 3 Temperature behavior with magnetic field parameter M.

2. Mathematical formulation

We ponder an electrically conducting, viscous, incompressible 2D dissipative ferrofluid flow over horizontally moving needle as displayed in Fig. 1. Here $(\bar{x}, \bar{r})$ represent the axial and radial coordinates in cylindrical form, respectively, where $\bar{c}$ is the thickness of the needle.

The size of the needle is thin, as its thickness is not more than the boundary layer formed on it. Also, the velocity of the horizontally moving thin needle is u_w. The flow governing equations using Tiwari and Das [19] nanofluid model in cylindrical coordinates are:

$$(\overline{ru})_{\bar{x}} + (\overline{rv})_{\bar{r}} = 0, \tag{1}$$

$$\rho_{nf}\{\bar{u}(\bar{u}_x) + \bar{v}(\bar{u}_r)\} = \mu_{nf}(1/\bar{r})\{\bar{r}(\bar{u}_r)\}_r - \sigma_{nf}B_0^2\bar{u}, \tag{2}$$

$$(\rho C_p)_{nf}\{\bar{u}(T_x) + \bar{v}(T_r)\} = k_{nf}(1/\bar{r})\{\bar{r}(T_r)\}_r + q''' + \sigma_{nf}B_0^2\bar{u}^2 + \mu_f(\bar{u}_r)^2, \tag{3}$$

the appropriate boundary restrictions are:

$$\left.\begin{aligned} &\bar{u} = u_0,\ \bar{v} = 0,\ T = T_0 \ at\ \bar{r} = R(\bar{x}) \\ &\bar{u} \to u_\infty,\ T \to T_\infty \text{ as } \bar{r} \to \infty \end{aligned}\right\}, \tag{4}$$

where $\bar{u}$ and $\bar{v}$ are the velocity components along axial and radial coordinates. And $R(x)$ represents the surface shape of the thin needle. The nanofluid parameters are given as

$$\left.\begin{aligned} &\frac{k_{nf}}{k_f} = \frac{(k_s+2k_f)-2\phi(k_f-k_s)}{(k_s+2k_f)+\phi(k_f-k_s)}, \frac{\sigma_{nf}}{\sigma_f} = \left(1 + \frac{3(\sigma-1)\phi}{(\sigma+2)-(\sigma-1)\phi}\right), \\ &\sigma = \frac{\sigma_p}{\sigma_f}, \rho_{nf} = \rho_f\{(1-\phi) + \phi(\rho_s/\rho_f)\}, \mu_{nf} = \mu_f(1-\phi)^{-2.5}, \\ &(\rho C_p)_{nf} = (\rho C_p)_f\{(1-\phi) + \phi(\rho C_p)_s/(\rho C_p)_f\} \end{aligned}\right\}, \tag{5}$$

to reduce the Eqs. (1)–(3) to the dimensionless form, the similarity transformations used are:

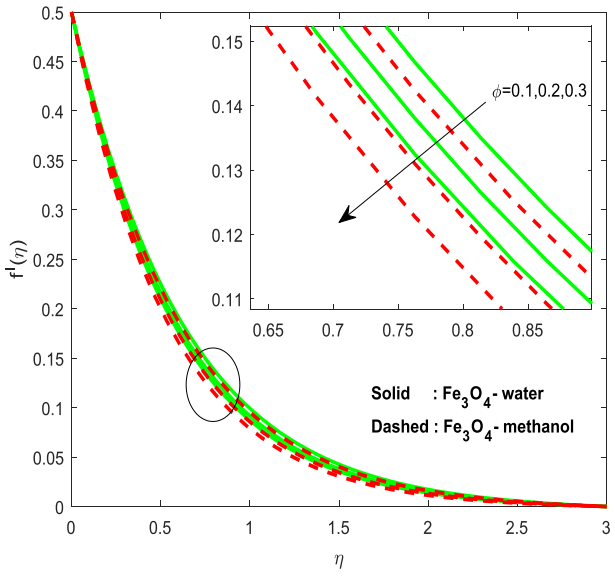

Fig. 4 Velocity behavior with volume fraction parameter ϕ.

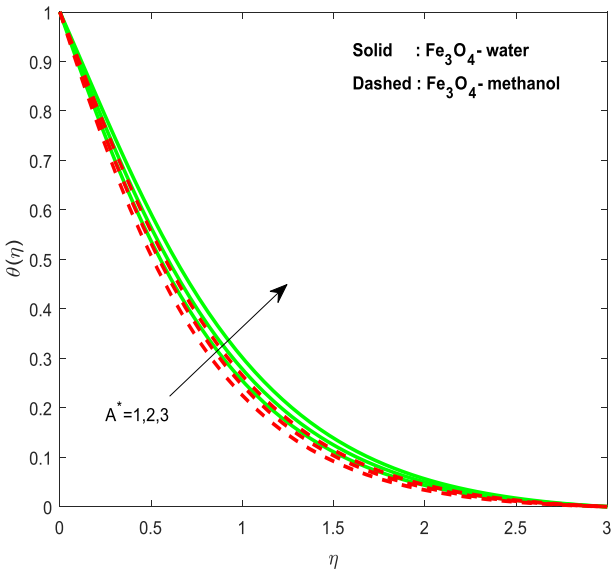

Fig. 6 Temperature behavior with A^*.

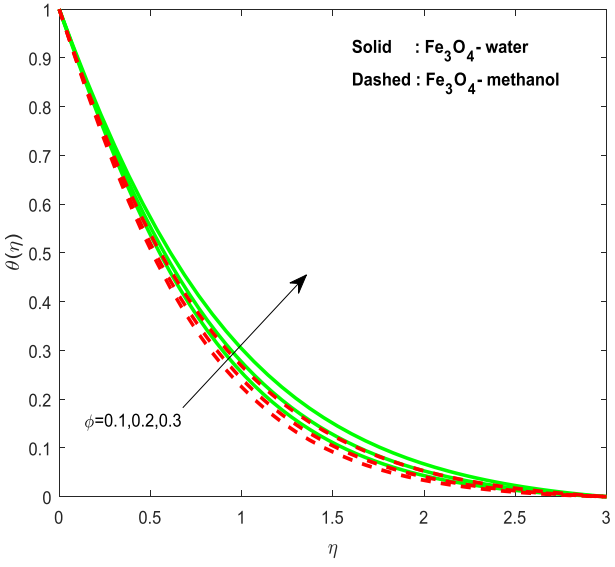

Fig. 5 Temperature behavior with volume fraction parameter ϕ.

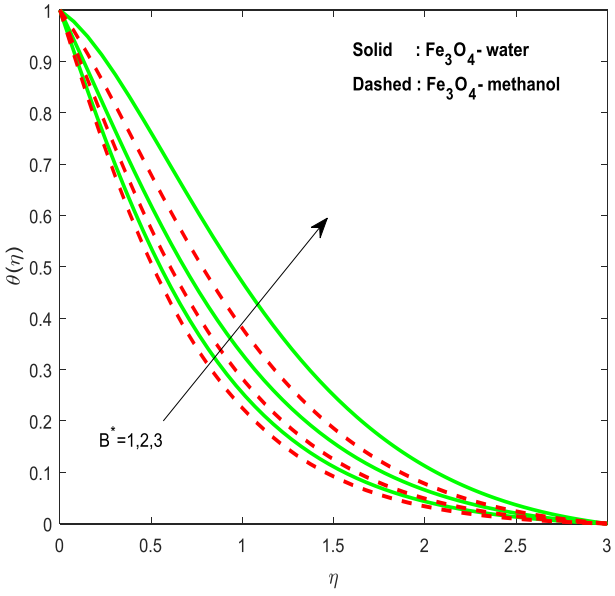

Fig. 7 Temperature behavior with B^*.

$$\left.\begin{aligned}&\psi = v_f\bar{x}f(\eta), \theta = (T-T_\infty)/(T_0-T_\infty), \eta = U_0\bar{r}^2/v_f\bar{x},\\ &\bar{u} = (1/\bar{r})\psi_r, \bar{v} = (-1/\bar{r})\psi_x, R(\bar{x}) = (v_f\overline{xc}/U)^{1/2},\\ &q''' = (k_fU_0(T_0-T\infty)/xv_f)\{A^*f' + B^*\theta\},\end{aligned}\right\} \quad (6)$$

By setting $\eta = \bar{c}$ in Eq. (6) describes the size and shape of the thin needle $\bar{r} = R(\bar{x})$.

Eq. (1) is automatically satisfied, further the Eqs. (2) and (3) reduced to:

$$(2Af'''\eta + 2Af'') + B(ff'' - Mf') = 0 \quad (7)$$

$$2K(\theta''\eta + \theta') + EPr\, f\theta' + (A^*f' + B^*\theta) + PrE_c(2\eta(f'')^2 + M(f')^2) = 0, \quad (8)$$

where

$$A = (1-\phi)^{-5/2}, B = 1-\phi+\phi(\rho_s/\rho_f), K = k_{nf}/k_f,$$
$$E = 1-\phi+\phi\{(\rho C_p)_s/(\rho C_p)_f\}, \quad (9)$$

transformed boundary conditions are:

$$\left.\begin{aligned}&f(\bar{c}) = (\gamma/2)\bar{c}, f'(\bar{c}) = \gamma/2, \theta(\bar{c}) = 1\\ &f'(\eta)\to(1-\gamma/2), \theta(\eta)\to\gamma/2 \ as\ \eta\to\infty\end{aligned}\right\}, \quad (10)$$

where "prime" denotes derivative w.r.t. η and the dimensionless parameters are expressed as,

$$M = \sigma_fB_0^2/2U_0\rho_f,\ Pr = \mu_fC_p/k_f,\ E_c = (2U_0)^2/C_p(T_0-T_\infty),\ \gamma = u_0/U_0,\ U_0 = u_0+u_\infty \quad (11)$$

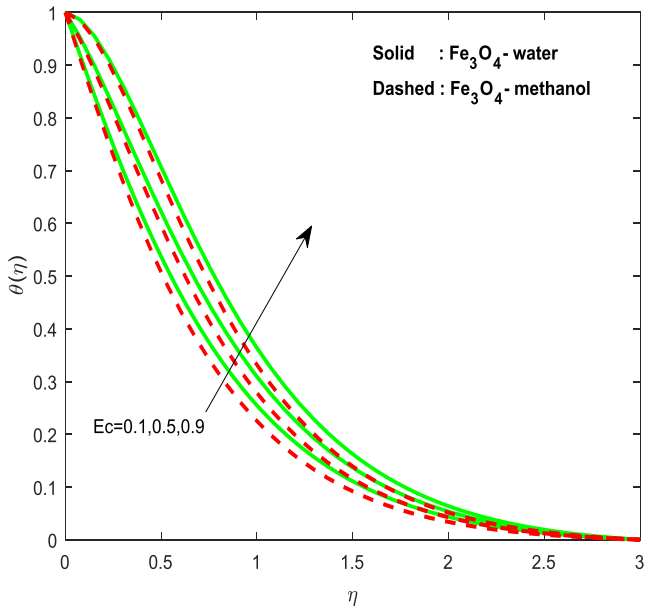

Fig. 8 Temperature behavior with viscous dissipation parameter E_c.

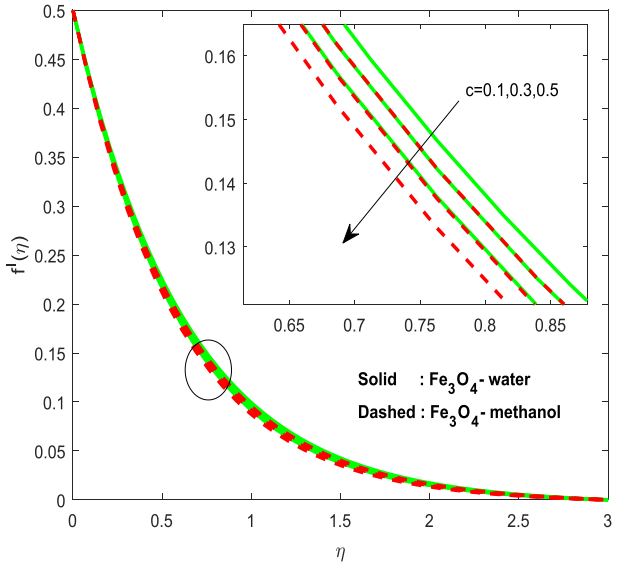

Fig. 9 Velocity behavior with needle thickness parameter $\bar{c}$.

The physical quantities of practical interest are C_f and Nu_x which are given by

$$C_f = \tau_w/\rho_f U_0^2, \;\; Nu_x = \bar{x}q_w/k_f(T_0 - T_\infty) \tag{12}$$

where τ_w and q_w, are given as:

$$\left.\begin{aligned} \tau_w &= \mu_{nf}(\bar{u}_{\bar{r}})_{\bar{r}=\bar{c}} = \mu_{nf}(4\bar{c}U_0^2/v_f\bar{x})f''(\bar{c}), \\ q_w &= -k_{nf}(T_{\bar{r}})_{\bar{r}=\bar{c}} = -k_{nf}\{2\bar{c}U_0(T_0 - T_\infty)/v_f\bar{x}\}\theta'(\bar{c}), \end{aligned}\right\} \tag{13}$$

Using Eq. (6), the above equation reduces as

$$Re_x^{1/2}C_f = 4\bar{c}^{1/2}Af''(\bar{c}), \;\; Re_x^{-1/2}Nu_x = -2\bar{c}^{1/2}K\theta'(\bar{c}) \tag{14}$$

where $Re_x = U_0\bar{x}/v_f$.

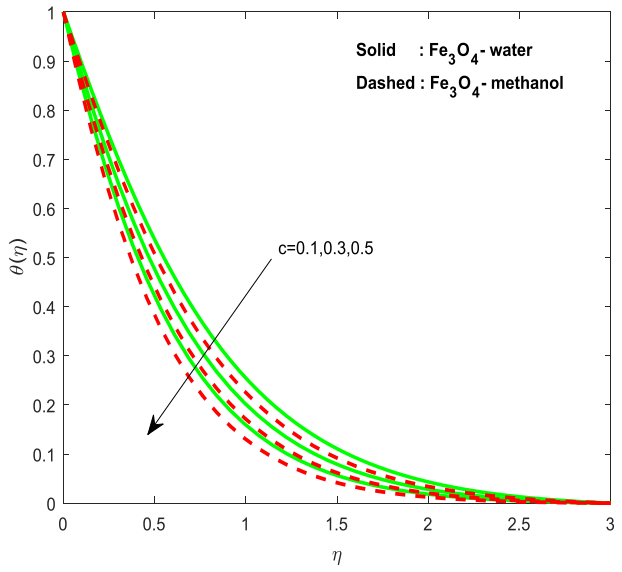

Fig. 10 Temperature behavior with needle thickness parameter $\bar{c}$.

3. Discussion of the results

Here we discuss the flow and energy transport behavior of two distinct ferrofluids under the influence of sundry physical parameters. The transformed dimensionless flow governing Eqs. (7) and (8) with associated corresponding boundary restrictions (10) are numerically solved by employing R-K and Newton methods. The impact of pertinent parameters viz. M, ϕ, A^*, B^*, E_c and $\bar{c}$ on flow and energy transport behavior of the fluid, with Nu_x and C_f are bestowed with the aid of graphs and tabular values. Certain parameter values are kept constant i.e. $\phi = 0.1$; $M = 1$; $\eta = 1$; $A^* = 1$; $B^* = 1$; $\lambda = 1$; $\bar{c} = 0.1$; $Pr = 6.587$ (water) and $Pr = 7.38$ (Methanol) in the complete study, excluding the changes are mentioned in Figs. 2–9 and Tables 2 and 3.

The impact of ascending values of M on temperature and velocity fields are portrayed in Figs. 2 and 3. We detect a decaying in velocity fields with M. Physically, this may happen because of the generation of Lorentz force (i.e. opposing force to the flow of ferrofluids). The existence of these force may lead to decline the fluid velocity and enlarges the thermal boundary layer thickness. Figs. 4 and 5 are depicted to observe the action of volume fraction parameter ϕ on velocity and temperature fields. From these figures, we noticed that the inflation in volume fraction parameter ϕ curtails the velocity fields but it inflates the thermal fields. Generally, as ϕ improves the viscosity of the fluid and then highly viscous fluid moves with lesser velocity. Hence we observe a declination in fluid velocity and enhancement in temperature fields. It is worth to mention that the water- Fe_3O_4 nanofluid has higher fluid temperature as compared with methanol- Fe_3O_4 nanofluids.

The nature of the temperature field for various values of A^* and B^* are displayed in Figs. 6 and 7. We may observe that the increasing values of A^* and B^* improves the fluid temperature. Generally, positive values of A^* and B^* produces heat and negative values of A^* and B^* absorbs heat. Hence it is found an improvement in fluid temperature. It is fascinating to write

Table 1 Thermo physical properties of water, methanol and Fe_3O_4.

Parameters	Water	Methanol	Fe_3O_4
ρ (Kg/m^3)	992	792	5180
C_p (J/Kg K)	4076	2545	670
k (W/mK)	0.605	0.2035	9.7
σ (S/m)	0.005	0.5×10^{-6}	0.74×10^{6}
Pr	6.587	7.38	–

that the thermal boundary thickness of water based ferrofluids is slightly higher than methanol based ferrofluids. Fig. 8 illustrates the impact of Ec on temperature fields. The figure reveals that the rising value of Ec improves the fluid velocity, this leads to increase in the fluid velocity near the surface and as a result friction heat will be produced. Because of this, we have seen enhancement in temperature field. Figs. 9 and 10 are constructed to study the impact of $\bar{c}$ on flow analysis. It is clearly seen that the improving values of $\bar{c}$ decelerates the profiles of the fluid flow.

Table 1 is drawn to display the thermophysical properties of base fluids and nanoparticles. Table 2 and 3 drawn to shed light on the response of Nu_x and C_f for various pertinent parameters for water- Fe_3O_4 ferrofluid and methanol- Fe_3O_4 ferrofluid, respectively. From above table, we found that, skin friction of water based ferrofluids are decelerated more than that of methanol based ferrofluids. Heat transfer rates can be controlled by A^* and B^*. The volume fraction of nanoparticles can improve the local Nusselt number effectively in Fe_3O_4 -

Table 2 Numerical values of C_f and Nu_x for Fe_3O_4-water nanofluid for various flow parameter values.

M	ϕ	A^*	B^*	E_c	c	Fe_3O_4-water	
						$f''(\bar{c})$	$-\theta'(\bar{c})$
1						−1.292476	0.852388
2						−1.536943	0.805100
3						−1.738413	0.766528
	0.1					−1.292476	0.852388
	0.2					−1.827584	1.043389
	0.3					−3.897519	1.596699
		1				−1.292476	0.852388
		2				−1.292476	0.757849
		3				−1.292476	0.663310
			1			−1.292476	0.852388
			2			−1.292476	0.593761
			3			−1.292476	0.191463
				0.1		−1.292476	0.852388
				0.5		−1.292476	0.439325
				0.9		−1.292476	0.026281
					0.1	−1.292476	0.852388
					0.3	−2.297010	1.819543
					0.5	−3.041710	2.794746

Table 3 Numerical values of C_f and Nu_x for Fe_3O_4-methanol nanofluid for various flow parameter values.

M	ϕ	A^*	B^*	E_c	$\bar{c}$	Fe_3O_4-methanol	
						$f''(\bar{c})$	$-\theta'(\bar{c})$
1						−1.323960	0.955844
2						−1.582287	0.900177
3						−1.794326	0.855024
	0.1					−1.323960	0.955844
	0.2					−1.900611	1.218736
	0.3					−4.118343	1.983086
		1				−1.323960	0.955844
		2				−1.323960	0.865306
		3				−1.323960	0.774793
			1			−1.323960	0.955844
			2			−1.323960	0.726384
			3			−1.323960	0.399975
				0.1		−1.323960	0.955844
				0.5		−1.323960	0.493412
				0.9		−1.323960	0.030980
					0.1	−1.323960	0.955844
					0.3	−2.356545	2.064814
					0.5	−3.125189	3.198403

Table 4 Validation of the numerical technique for Nu_x.

M	*RKN*	*RKF*	*RKS*	*BVP4C*	*BVP5C*
1	0.955844	0.9558444521	0.9558444521	0.9558444521	0.9558444521
2	0.900177	0.9001772133	0.9001772134	0.9001772134	0.9001772134
3	0.855024	0.8550247642	0.8550247641	0.8550247641	0.8550247642
4	0.803241	0.8032416430	0.8032416430	0.8032416432	0.8032416432

methanol ferrofluid as compared with the Fe_3O_4 -water ferrofluid. Eckert number Ec has a tendency to decline the local Nusselt number. Table 4 shows the validation of the computational results by comparing with the other techniques.

4. Conclusions

The 2D boundary layer flow of water and methanol based ferrofluids with non-uniform heat generation/absorption and viscous dissipation is numerically analysed. The electrical conductivity of ferrofluid is taken into consideration. A few important findings of the present study are listed below.

- A significant hike in heat transfer performance can be delivered in methanol based ferrofluid when compared to water based ferrofluid.
- Thermal boundary layer thickness of water-Fe_3O_4 ferrofluid is higher than the methanol-Fe_3O_4 ferrofluid.
- Water based Fe_3O_4 ferrofluid moves faster than the methanol based Fe_3O_4 nanofluid.
- The parameters A^* and B^* acts as a heat transfer rate controlling parameters.
- The parameter ϕ improves the local Nusselt number of Fe_3O_4 -methanol ferrofluid when compared with Fe_3O_4 -water ferrofluid.

Acknowledgement

The authors acknowledge the UGC for financial support under the UGC Dr. D. S. Kothari Postdoctoral Fellowship Scheme (No.F.4-2/2006 (BSR)/MA/13-14/0026).

References

[1] A.J. Chamkha, C. Issa, Effects of heat generation/absorption and thermophoresis on hydromagnetic flow with heat and mass transfer over a flat surface, Int. J. Numer. Methods Heat Fluid Flow 10 (4) (2000) 432–449.
[2] A.K. Da Silva, L. Gosselin, Optimal geometry of L and C-shaped channels for maximum heat transfer rate in natural convection, Int. J. Heat Mass Transf. 48 (3) (2005) 609–620.
[3] A. Ali, N. Amin, I. Pop, The unsteady boundary layer flow past a circular cylinder in micropolar fluids, Int. J. Numer. Methods Heat Fluid Flow 17 (7) (2007) 692–714.
[4] U. Khan, N. Ahmed, S. Tauseef, Analysis of magnetohydrodynamic flow and heat transfer of Cu – water nanofluid between parallel plates for different shapes of nanoparticles, Neural Comput. Appl. (2016), http://dx.doi.org/10.1007/s00521-016-2596-x.
[5] N. Ahmed, S.T. Mohyud-din, S.M. Hassan, Flow and heat transfer of nanofluid in an asymmetric channel with expanding and contracting walls suspended by carbon nanotubes: A Numerical Investigation, Aerosp. Sci. Technol. (2015), http://dx.doi.org/10.1016/j.ast.2015.10.022.
[6] M. Sheikholeslami, Influence of Lorentz forces on nanofluid flow in a porous cylinder considering Darcy model, J. Mol. Liq. (2016), http://dx.doi.org/10.1016/j.molliq.2016.11.022.
[7] C. Sulochana, G.P. Ashwinkumar, N. Sandeep, Numerical investigation of chemically reacting MHD flow due to a rotating cone with thermophoresis and Brownian motion, Int. J. Adv. Sci. Technol. 86 (2016) 61–74.
[8] N. Sandeep, M.G. Reddy, Heat transfer of nonlinear radiative magnetohydrodynamic Cu-water nanofluid flow over two different geometries, J. Mol. Liq. 225 (2017) 87–94.
[9] L.L. Lee, Boundary layer over a thin needle, Phys. Fluids 10 (1967) 820.
[10] J.P. Narain, M.S. Uberoi, Forced heat transfer over thin needles, J. Heat Transfer 94 (1972) 240–242.
[11] S.L. Lee, T.S. Chen, B.F. Armaly, Mixed convection along vertical cylinders and needles with uniform surface heat flux, J. Heat Transfer 109 (1987) 711.
[12] S. Ahmad, N.M. Arifin, R. Nazar, I. Pop, Mixed convection boundary layer flow along vertical thin needles: Assisting and opposing flows, Int. Commun. Heat Mass Transf. 35 (2) (2008) 157–162.
[13] C. Sulochana, N. Sandeep, Dual solutions for radiative MHD forced convective flow of a nanofluid over a slendering stretching sheet in porous medium, J. Nav. Archit. Mar. Eng. 12 (2015) 115–124.
[14] U. Khan, N. Ahmed, S.T. Mohyud-din, Numerical investigation for three dimensional squeezing flow of nanofluid in a rotating channel with lower stretching wall suspended by carbon nanotubes, Appl. Therm. Eng. (2016), http://dx.doi.org/10.1016/j.applthermaleng.2016.11.104.
[15] U. Khan, N. Ahmed, S.T. Mohyud-din, Thermo-diffusion, diffusion-thermo and chemical reaction effects on MHD flow of viscous fluid in divergent and convergent channels, Chem. Eng. Sci. (2015), http://dx.doi.org/10.1016/j.ces.2015.10.032.
[16] M. Jayachandra Babu, N. Sandeep, MHD non-Newtonian fluid flow over a slendering stretching sheet in the presence of cross-diffusion effects, Alexandria Eng. J. 55 (2016) 2193–2201.
[17] S.U.S. Choi, Enhancing thermal conductivity of fluids with nanoparticles, ASME Pub. 231 (1995) 99–106.
[18] J. Buongiorno, Convective transports in nanofluids, ASME J. Heat Transfer 128 (2006) 240–250.
[19] R.K. Tiwari, M.K. Das, Heat transfer augmentation in a two-sided lid-driven differentially heated square cavity utilizing nanofluids, Int. J. Heat Mass Transf. 50 (2007) 2002–2018.
[20] S. Zulfiqar, A. Zaidi, S.T. Mohyud-din, Convective heat transfer and MHD effects on two dimensional wall jet flow of a nanofluid with passive control model, Aerosp. Sci. Technol. (2015), http://dx.doi.org/10.1016/j.ast.2015.12.008.

[21] M. Hassani, M.M. Tabar, H. Nemati, G. Domairry, F. Noori, An analytical solution for boundary layer flow of a nanofluid past a stretching sheet, Int. J. Therm. Sci. 50 (2011) 2256–2263.
[22] S.K. Soid, A. Ishak, I. Pop, Boundary layer flow past a continuously moving thin needle in a nanofluid, Appl. Therm. Eng. 114 (2017) 58–64.
[23] M. Sheikholeslami, A. Zeeshan, Analysis of flow and heat transfer in water based nanofluid due to magnetic field in a porous enclosure with constant heat flux using CVFEM, Comput. Methods Appl. Mech. Engrg. (2017), http://dx.doi.org/10.1016/j.cma.2017.03.024.
[24] W. Ibrahim, B. Shankar, MHD boundary layer flow and heat transfer of a nanofluid past a permeable stretching sheet with velocity, thermal and solutal slip boundary conditions, Comput. Fluids 75 (2013) 1–10.
[25] N. Sandeep, B.R. Kumar, M.S.J. Kumar, A comparative study of convective heat and mass transfer in non-Newtonian nanofluid flow past a permeable stretching sheet, J. Mol. Liq. 212 (2015) 585–591.
[26] M.S. Abdel-wahed, E.M.A. Elbashbeshy, T.G. Emam, Flow and heat transfer over a moving surface with non-linear velocity and variable thickness in a nanofluids in the presence of Brownian motion, Appl. Math. Comput. 254 (2015) 49–62.
[27] C. Sulochana, G.P. Ashwinkumar, N. Sandeep, Similarity solution of 3D Casson nanofluid flow over a stretching sheet with convective boundary conditions, J. Niger. Math. Soc. 35 (2016) 128–141.
[28] M. Sheikholeslami, Influence of magnetic field on nanofluid free convection in an open porous cavity by means of Lattice Boltzmann Method, J. Mol. Liq. (2017), http://dx.doi.org/10.1016/j.molliq.2017.03.104.
[29] I.L. Animasaun, N. Sandeep, Buoyancy induced model for the flow of 36nm alumina-water nanofluid along upper horizontal surface of a paraboloid of revolution with variable thermal conductivity and viscosity, Powder Technol. 301 (2016) 858–867.
[30] M. Sheikholeslami, Numerical simulation of magnetic nanofluid natural convection in porous media, Phys. Lett. A (2017), http://dx.doi.org/10.1016/j.physleta.2016.11.042.
[31] M.J. Babu, N. Sandeep, Three-dimensional MHD slip flow of nanofluids over a slendering stretching sheet with thermophoresis and Brownian motion effects, Adv. Powder Technol. 27 (5) (2016) 2039–2050.
[32] U. Khan, N. Ahmed, S. Tauseef, Heat transfer effects on carbon nanotubes suspended nanofluid flow in a channel with non-parallel walls under the effect of velocity slip boundary condition : a numerical study, Neural Comput. Appl. (2015), http://dx.doi.org/10.1007/s00521-015-2035-4.
[33] C. Sulochana, G.P. Ashwinkumar, N. Sandeep, Transpiration effect on stagnation-point flow of a Carreau nanofluid in the presence of thermophoresis and Brownian motion, Alexandria Eng. J. 55 (2016) 1151–1157.
[34] M. Sheikholeslami, M. Sadoughi, Mesoscopic method for MHD nanofluid flow inside a porous cavity considering various shapes of nanoparticles, Int. J. Heat Mass Transf. 113 (2017) 106–114.
[35] N. Sandeep, Effect of Aligned Magnetic field on liquid thin film flow of magnetic-nanofluid embedded with graphene nanoparticles, Adv. Powder Technol. 28 (2017) 865–875.
[36] M. Sheikholeslami, Influence of Coulomb forces on Fe_3O_4 - H_2O nanofluid thermal improvement, Int. J. Hydrogen Energy (2016) 1–9, http://dx.doi.org/10.1016/j.ijhydene.2016.09.185.